POLITECNICO DI TORINO
Repository ISTITUZIONALE

Iron Losses and Parameters Investigation of Multi-Three-Phase Induction Motors in Normal and Open-Phase Fault Conditions

(Article begins on next page)

26 April 2024

Iron Losses and Parameters Investigation of Multi-Three-Phase Induction Motors in Normal and Open-Phase Fault Conditions

Ornella Stiscia, *Student Member, IEEE*, Marco Biasion, *Student Member, IEEE*,
Sandro Rubino, *Member, IEEE*, Silvio Vaschetto, *Senior Member, IEEE*,
Alberto Tenconi, *Senior Member, IEEE*, and Andrea Cavagnino, *Fellow, IEEE*

Abstract -- Among multi-phase solutions, multi-three-phase induction machines (IMs) are gaining an increasing interest in the industry due to their advantages to be configured as multiple three-phase units simultaneously on the same magnetic circuit. According to this scenario, the identification of the equivalent circuit parameters and conventional iron losses covers a key role in evaluating performance and efficiency, especially when the machine is operated in a wide torque-speed range. Therefore, the goal of this paper is to investigate the core losses and the saturation phenomena of multi-three-phase IMs operated in normal and open-three-phase fault conditions under different harmonic contents of the air-gap magnetomotive force. A procedure to identify the parameters of the equivalent circuit of the machine in faulty conditions is reported. Experimental results are presented on a 12-phase asymmetrical IM featuring a quadruple three-phase stator winding. Finally, a comparison between normal and faulty conditions in terms of efficiency and losses for several machine working points is reported.

Index Terms-- multi-phase induction machines, iron losses, parameters identification, standard tests.

I. INTRODUCTION

MULTIPHASE machines present several advantages compared to their three-phase counterparts. Especially in high-power applications, the stator current level is reduced as the number of phases increases. Furthermore, multi-phase machines are preferred in safety-critical scenarios due to their fault-tolerant capability, representing a consolidated solution in applications like ships and aircraft [1]. In this context, multi-three-phase machines are experiencing significant interest from the industry since the stator is configured with multiple three-phase winding sets operating simultaneously. Each set is fed with a three-phase power converter, allowing the adoption of consolidated three-phase technologies. In this way, costs and design efforts of the system are significantly reduced.

The detailed knowledge of the equivalent circuit parameters of multi-three-phase induction machines (IMs) is essential for an accurate analysis of their performance in normal and faulty conditions, i.e., when all the three-phase sets are active or the loss of one or more of them occurs. Although the literature reports many contributions to the parameter identification of three-phase IMs, very few efforts have focused on multi-three-phase IMs in normal and open-winding fault conditions [2]. In [3], using zero-sequence models, an online estimation technique for the stator resistance and the stator leakage inductance in symmetrical six-phase machines was presented. A similar methodology was developed in [4], discussing the parameter identification of generic multi-phase IMs. The magnetic model of multi-phase IMs operated in normal and faulty conditions was investigated in [5] for subsequent selection of the optimal operating flux level. However, most of the methods mentioned above consider inverter-fed machines, affecting the estimation of the equivalent circuit parameters due to the nonlimnearities related to the distorted supply. In multi-three-phase IMs, as in their three-phase counterparts, the conventional iron losses estimated by the standard no-load test procedure account for the magnetic losses in the core (i.e., hysteresis and eddy current losses) as well as the losses due to secondary effects, e.g., harmonic Joule losses in the rotor cage. However, when multi-three-phase IMs operate in faulty conditions, the conventional iron losses may change because of the different harmonic content of the spatial distribution of the air gap MMF. The accurate estimation of such loss contribution is not straightforward. Moreover, it represents an essential aspect for accurately predicting the machine performance in the whole speed-torque range, especially at high operating speed.

This paper investigates conventional iron losses and saturation phenomena in the parameters identification and nonlinearities of multi-three-phase IMs when operated in normal and open-winding fault conditions (open-three-phase fault event) under "*pure*" sinusoidal supply. The standard no-load and locked-rotor tests are carried out on a 12-phase asymmetrical IM, rated 10 kW at 6000 rpm. The machine is fed with a multi-three-phase sinusoidal power supply to avoid the nonlinearities introduced by the deadtime of the pulse-width modulation (PWM) of inverters on the parameter's estimation, especially the iron losses. The paper reports an in-depth analysis of the harmonic content of the air gap MMF in normal and different faulty conditions. Finally, the efficiency based on the measured parameters of the considered multi-three-phase IM is computed in normal and open-winding fault conditions at different operating points, using a developed efficiency mapping for IM multi-three-phase machines.

The authors are with Dipartimento Energia "G. Ferraris", Politecnico di Torino, 10129 Torino, Italy
(e-mail: ornella.stiscia@polito.it, marco.biasion@polito.it, sandro. rubino@polito.it, silvio.vaschetto@polito.it, andrea. cavagnino@polito.it, alberto.tenconi@polito.it).
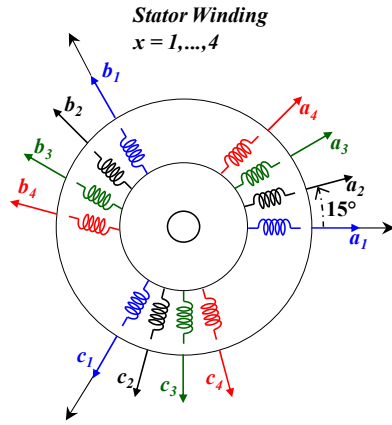
Fig. 1. A view of the magnetic axes of the asymmetrical 12-phase IM.

Therefore, showing how the proposed analysis is pivotal to understanding the performance of multi-three-phase IM operated in wide torque-speed ranges and with one or more three-phase sets in faulty conditions.

II. CASE OF STUDY: THE QUADRUPLE-THREE-PHASE IM

The machine considered in this paper is an asymmetrical 12-phase IM featuring a quadruple-three-phase (4 sets) configuration of the stator winding, rated 10 kW at 6000 rpm. The sketch of the magnetic axes of the machine windings is shown in Fig. 1. The machine has four poles, 1 slot/pole/phase and 19 conductors per slot. Thus, the single layer winding is inserted in 48 stator slots. The distribution of the conductors in the stator slots is shown in Fig. 2. When the machine operates in open-three-phase fault conditions, the conductors are not supplied.

Multi-three-phase machines can be modelled mainly using two mathematical approaches presented in the literature. The first one, called Multi Stator (MS), considers the multi-phase stator winding as multiple three-phase windings, while the rotor cage is modeled as an equivalent three-phase winding. This approach decomposes the space of the machine variables in multiple parallel time-fundamental models, thus applying a dedicated Clarke transformation to each three-phase winding set [6]. This approach highlights the contributions to the machine flux and torque provided by each three-phase winding set, and it is particularly suited for implementing modular control schemes. The advantage of this modeling approach is the possibility to consider an individual and independent control for all the winding sets; hence, the power/current sharing among the different units is easily achieved. On the other hand, this multiple dq modeling approach leads to a significant cross-coupling effect among the equations of the different three-phase winding sets [7]. It also does not offer clear insights about the machine operation and harmonic mapping [8]. For the 12-phase machine under study, the MS approach defines four different stator flux linkage and current vectors. The electromagnetic torque results from the contribution of the four stator sets interacting with the equivalent three-phase rotor winding (rotor cage).

The second modeling approach, known as Vector Space Decomposition (VSD), decomposes the space of the machine
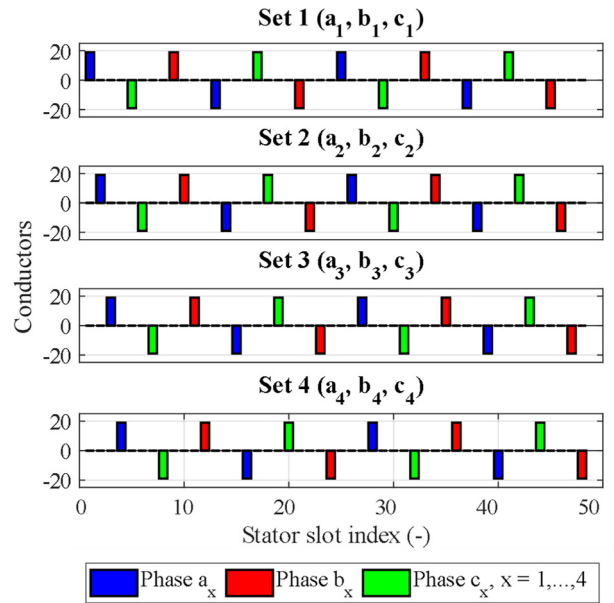

Fig. 2. Conductors' distribution of the 12-phase IM.

variables into multiple decoupled subspaces [9], [10]. This approach is very useful because it provides a general view of the machine. The number of decoupled subspaces is equal to $n_{ph}/2$, and this is achieved by using an $n_{ph} \times n_{ph}$ transformation matrix, where n_{ph} is the number of phases of the stator winding [8]. Through this approach, the flux and torque production can be modeled as an equivalent three-phase machine in the fundamental subspace ($\alpha\beta$) by using the well-known VSD transformation [11]. Nevertheless, there is no possibility to distinguish the contribution of each set to the total flux linkage and electromagnetic torque of the machine. Indeed, the remaining VSD subspaces represent the harmonics and zero-sequence model of the machine that do not provide any contribution to the electromechanical energy conversion.

Therefore, for the machine under study ($n_{ph} = 12$ in asymmetrical configuration with $\pi/12$ spatial shift), it is necessary to define six subspaces: the main subspace (α,β), the harmonic subspaces (x_5,y_5), (x_7,y_7), (x_{11},y_{11}), and four zero-sequence components ($0_1,0_2,0_3,0_4$). The VSD approach leads to the equivalent circuit shown in Fig. 3, which considers the main (α,β) subspace responsible for the flux and torque production in the machine. For this reason, the VSD approach was considered the most convenient for the purposes of the research carried out in this paper.

Practically, with the VSD approach, the authors consider an equivalent three-phase machine, and the variables of the associated equivalent circuit are computed by averaging out the values belonging to each of the active three-phase sets (12 phases in 4 three-phase sets for the machine under study). Indeed, it is possible to estimate the machine parameters, including the conventional iron losses, by performing the conventional no-load and locked-rotor tests, as for three-phase machines. The postprocessing of the test results provides all the necessary information to predict the machine performance in both normal and open-winding fault conditions.
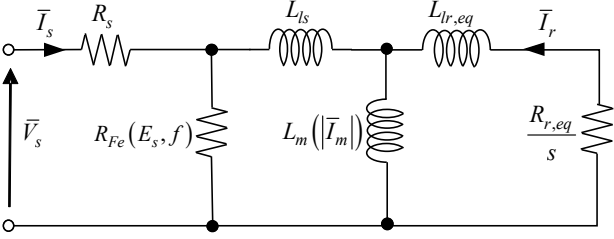
Fig. 3. Equivalent VSD circuit of the machine in the main subspace in the stationary reference frame (αβ).

Concerning the equivalent circuit in Fig. 3, R_s and L_{ls} stand for the stator winding resistance and leakage inductance, which do not depend on the number of active sets; $L_{m,eq}$, is the equivalent magnetizing inductance; $L_{lr,eq}$, $R_{r,eq}$ are the the equivalent rotor leakage inductance and the equivalent rotor resistance converted to the stator side, respectively. The values of the equivalent parameters depend on the number of active sets. Finally, R_{Fe} stands for the equivalent iron loss resistance, which depends again on the number of active sets, the supply frequency f and the machine back-emf E_s.

The magnetizing inductance decreases when disconnecting one or more sets. Indeed, a more magnetizing current is necessary to provide a given magnetizing flux as the number of active three-phase sets is reduced. For this reason, the equivalent magnetizing inductance $L_{m,eq}$ is computed as (1) also suitable in saturation conditions.

$$L_{m,eq} = L_m \cdot \frac{n_{ON}}{4} \qquad (1)$$

L_m is the magnetizing inductance measured in normal conditions (4 sets ON), while n_{ON} is the number of active sets.

The same rescaling procedure as in (1) can be used to calculate the equivalent rotor resistance and the equivalent rotor leakage inductance referred to the stator side as:

$$L_{lr,eq} = L_{lr} \cdot \frac{n_{ON}}{4}, \qquad R_{r,eq} = R_r \cdot \frac{n_{ON}}{4} \qquad (2)$$

The rescaling procedure described above is not valid for the conventional iron losses.

A. MMF Distribution in Normal and Faulty conditions

This subsection analyses the stator MMF distribution in normal and faulty conditions for multi-three-phase machines [12]. Under the assumptions of ideal magnetic cores ($\mu_{Fe} \rightarrow \infty$) and an infinitesimal slot opening, it is simple to determine the air-gap MMF step-like distribution summing the contribution of each three-phase set. The MMF distribution can be computed as:

$$MMF(\alpha,t) = \sum_{x=1,2,3,4} \left[\sum_{h=6k+1} \frac{3}{2} \hat{I}_m \frac{Z_f k_{w,h}}{hp\pi} \sin\left(hp\alpha - \omega t - (x-1)\frac{(h-1)\pi}{12} \right) \right] \qquad (3)$$

where $\hat{I}_m$ is the peak value of the magnetizing phase current, Z_f is the number of conductors in series per phase, $k_{w,h}$ is the harmonic winding factor (equal to 1 for each harmonic because the winding has been distributed using 1 slot/pole/phase), p is the pole pair number, h is the harmonic index ($h = 1$ for the fundamental four-pole distribution), x is the set index and $k = 0, \pm1, \pm2, \dots \pm\infty$.

When all the four three-phase sets are active, (3) can be simplified in (4), where it is possible to observe that only the tooth harmonics are present in the MMF harmonic spectrum.

TABLE I: SPATIAL VECTOR DIAGRAMS OF THE AIR-GAP MMF HARMONICS FOR THE QUADRUPLE THREE-PHASE WINDING

Set 1, *Set* 2, *Set* 3, *Set* 4

$$MMF(\alpha,t) = 6 \cdot \hat{I}_m \sum_{h=24k+1} \frac{Z_f k_{w,h}}{hp\pi} \sin(hp\alpha - \omega t) \qquad (4)$$

However, (3) is more general and it can be used to better investigate the MMF harmonic spectrum fault conditions of one or more three-phase sets. For the purpose, it is useful to represent each MMF harmonic of a three-phase winding as a spatial vector, where the shift angle between the vectors must be defined considering the harmonic order h with its correct sign. The sketch of these vector diagrams is shown in Table I, where the color is used to identify the set, like in Fig. 1. In this table the amplitude of the harmonics is not in scale for readability reasons.

Looking at Table I, it is evident that when all the three-phase sets are supplied with the same magnetizing current, all the harmonic sums are equal to zero with the obvious exception of the fundamental and the tooth harmonics (i.e. $h = 23$ and $h = 25$). As an example, in the case of the faults of the second set (the Set 2 in Fig. 1), the black dashed arrow disappears and the harmonic sums are no longer equal to zero for all the harmonics orders. It is interesting to observe that for a fault of two sets, different MMF harmonics can be present in the air-gap if the two active sets are shifted of 15 or 30 electrical degrees, respectively. The step-like MMF waveforms for selected working conditions of the quadruple-three-phase winding are reported in Fig. 4 - Fig. 7, while their harmonic contents are computed Table II to Table V. Having assumed the problem magnetically linear, the MMF harmonics have been calculated using $\hat{I}_m = 1$ A. With respect to the lower order MMF harmonics (i.e. the belt harmonic $h = 5$ and $h = 7$), in absolute terms the most severe case is the considered two-sets fault (see Table IV), while the one-set and the three-sets faults are substantially comparable. It is also interesting to observe that the 23rd and 25th tooth harmonics decrease with the increase of the number of the faulty sets. In fact, also the fundamental components show the same trend.
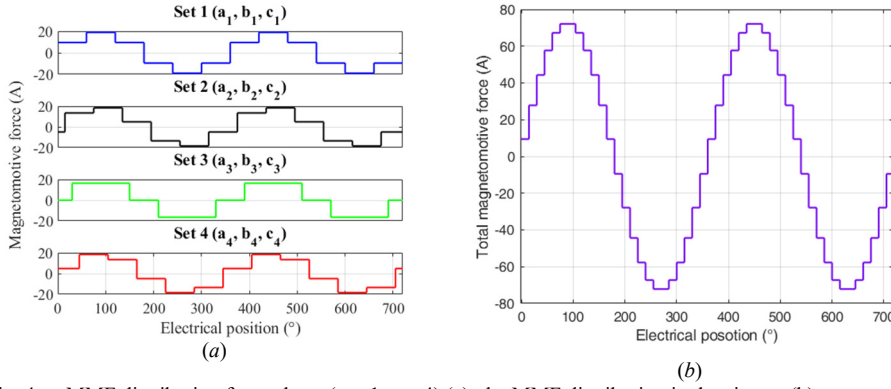
Fig. 4. MMF distribution for each set (x = 1, …, 4) (a), the MMF distribution in the air-gap (b), and the harmonic content of the MMF (Table II) with four active sets.

TABLE II: HARMONIC CONTENT OF THE MMF DISTRIBUTION (4 ACTIVE SETS)

Harmonic order (-)	Magnitude (%)
1	72.6 A (100 %)
5	0 %
7	0 %
11	0 %
13	0 %
17	0 %
19	0 %
23	3.1 A (4.3%)
25	2.9 A (4.0%)

Fig. 5. MMF distribution for each set (x= 1, …, 4) (a), the MMF distribution in the air-gap (b), and the harmonic content of the MMF (Table III) with three active sets.

TABLE III: HARMONIC CONTENT OF THE MMF DISTRIBUTION (SET 1, SET 2 AND SET 3 ACTIVE)

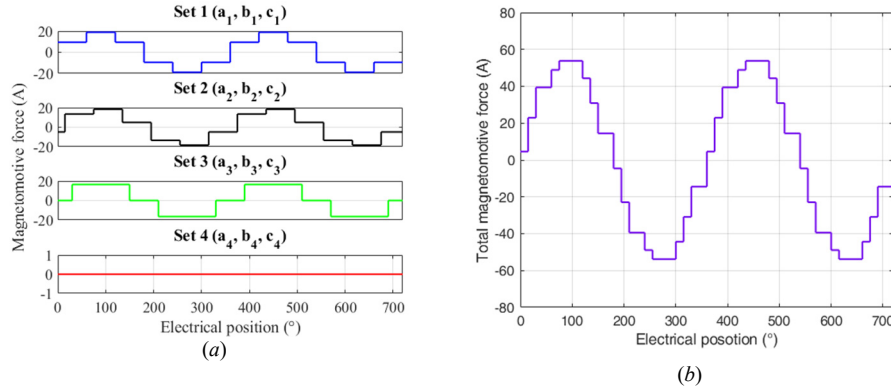| Harmonic order (-)	Magnitude (%)
1	54.4 A (100%)
5	3.6 A (6.7 %)
7	2.6 A (4.8 %)
11	1.6 A (3.0 %)
13	1.4 A (2.6 %)
17	1.1 A (2.0 %)
19	1.0 A (1.8 %)
23	2.3 A (4.3%)
25	2.2 A (4.0%)

Fig. 6. MMF distribution for each set (x= 1, …, 4) (a), the MMF distribution in the air-gap (b), and the harmonic content of the MMF (Table IV) with two active sets.

TABLE IV: HARMONIC CONTENT OF THE MMF DISTRIBUTION (SET 1 AND SET 2 ACTIVE)

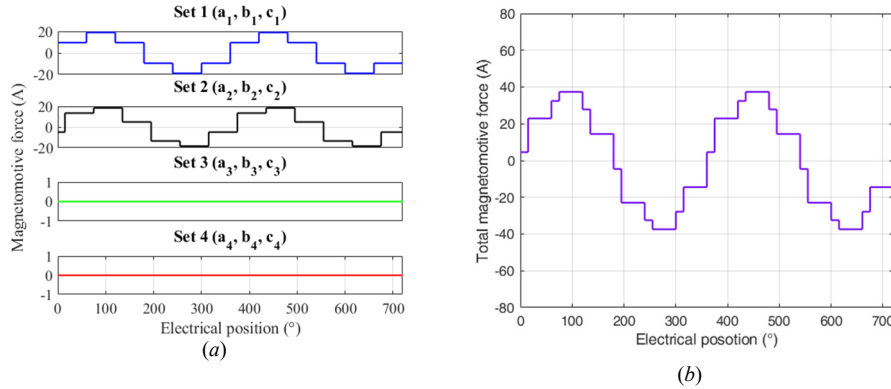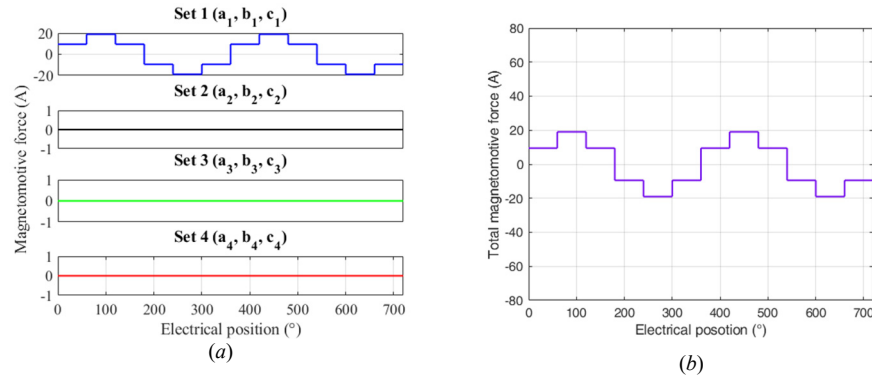| Harmonic order (-)	Magnitude (%)
1	36.6 A (100%)
5	5.1 A (14.0%)
7	3.6 A (10.0%)
11	0 A (0%)
13	0 A (0%)
17	1.5A (4.2%)
19	1.3A (3.7%)
23	1.6 A (4.3%)
25	1.4 A (4.0%)

Fig.7. MMF distribution for each set (x= 1, …, 4) (a), the MMF distribution in the air-gap (b), and the harmonic content of the MMF (Table V) with one active set.

TABLE V: HARMONIC CONTENT OF THE MMF DISTRIBUTION (1 ACTIVE SET)

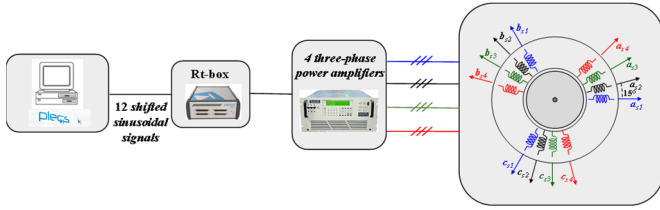| Harmonic order (-)	Magnitude (%)
1	18.1 A (100%)
5	3.6 A (20.0 %)
7	2.6 A (14.3 %)
11	1.6 A (9.1%)
13	1.4 A (7.7%)
17	1.1 A (5.9 %)
19	1.0 A (5.3 %)
23	0.8 A (4.3%)
25	0.7 A (4.0%)

Fig. 8. Sketch of the test rig used for parameter measurement.

III. MODEL PARAMETER MEASUREMENTS

No-load and locked-rotor tests under sinusoidal supply were performed using an open-loop voltage/frequency algorithm (V/Hz) implemented on the real-time control prototyping board PLECS RT-BOX 1 – see Fig. 8. The reference voltage signals were applied to four independent three-phase power sources operated as linear power amplifiers and synchronized to each other. The electrical quantities at the machine terminals were recorded using high-accuracy digital power meters in Aron configuration for each three-phase winding set since these operate with an isolated star-point. The tests allowed to account for the following nonidealities considered in the equivalent circuit of Fig. 3:

- the saturation effect on the magnetizing inductance L_m, which profile depends on the number of active sets;
- the impact of the frequency and the number of active sets on the equivalent rotor resistance $R_{r,eq}$;
- the impact of the number of active sets on the equivalent locked-rotor inductance L_{cc}, i.e., $L_{ls} + L_{lr,eq}$;
- the influence of the frequency and the stator voltage on the equivalent iron loss resistance R_{Fe}, depending on the machine operating conditions (normal or open-winding fault).

From the no-load operation of the machine, it is possible to estimate the conventional iron losses. Here, the nomenclature '*conventional*' refers to the iron losses measured by the standard no-load test procedures that account for the magnetic losses in the core (i.e., hysteresis and eddy current losses) as well as the additional losses due to secondary effects, e.g., harmonic Joule losses in the rotor cage [13]. These additional harmonic losses are not load-dependent; thus, they are 'automatically' included in the measured conventional iron losses. In this way, they can also be used for estimating the machine's efficiency in different load conditions. The conventional iron losses $P_{c,Fe}$ can be estimated from the power balance of the machine operating at no-load as in (5).

$$P_{c,Fe} = P_{no-load} - n_{ph} \cdot R_s \cdot I_0^2 - P_{mech0} \qquad (5)$$

where $P_{no-load}$, P_{mech0} and I_0 are the no-load active power, the mechanical losses and the no-load stator current, respectively.

Fig. 9 shows the parameters of the equivalent circuit that are subjected to the rescaling based on the number of active sets and whose description is reported in Section II. In Fig. 9a, the magnetizing inductance of the machine in all four different operating conditions is reported. In saturated conditions, the no-load current measured with one active set is higher than that in normal conditions by a factor $4/n_{on}$. The magnetizing profiles confirm (1), and applying a scaling factor $n_{on}/4$, the profiles are overlapped.
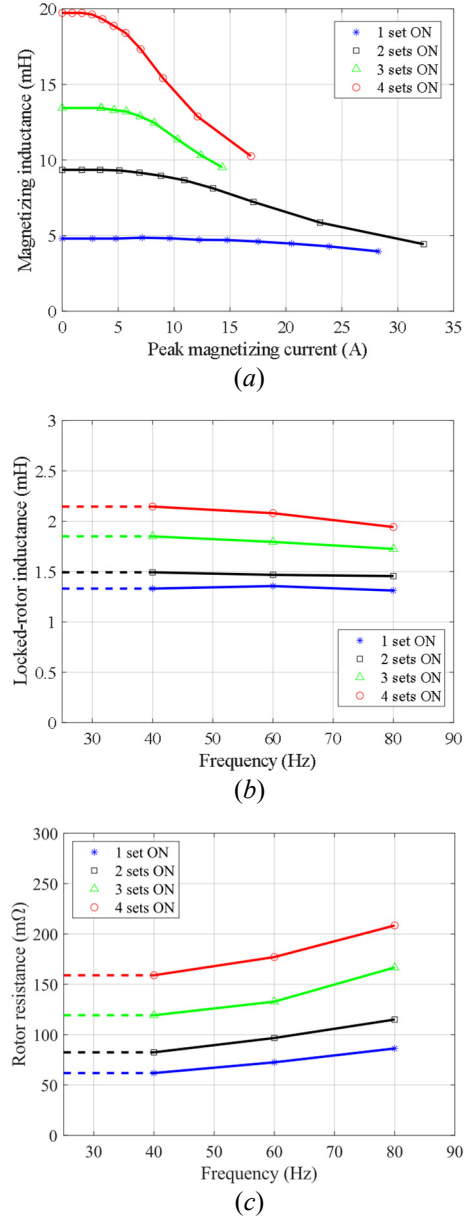

(a)

(b)

(c)

Fig. 9. The equivalent magnetizing inductance (a), locked-rotor inductance (b), and rotor resistance (c) for different winding configurations.

The profiles of locked- rotor inductance L_{cc} and the rotor resistance R_r in normal and open-winding fault conditions, both evaluated with the locked-rotor tests, are reported in Fig. 9b and Fig. 9c, respectively.

In Fig. 9b, the profiles of the locked- rotor inductance are shown: its value decreases as the number of faulty winding sets increases, as already highlighted in (2). In contrast, the stator leakage inductance L_{ls} is not influenced by the number of active sets [4].

In order to determine the rotor resistance as a function of the frequency (to account for the skin effect in the rotor cage), the locked-rotor tests were performed by limiting the supply frequency in the range from 40 Hz to 80 Hz. The maximum value for the test frequency was determined to be 80 Hz according to the operative values of the tested IM [14]. In this way, the skin effect on the stator winding resistance is practically always negligible.
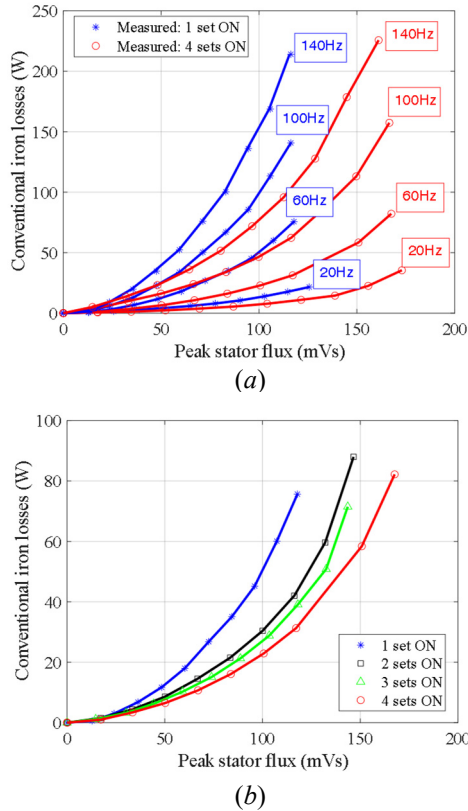
Fig. 10. Iron losses for one and four active sets at different frequencies (a) and iron losses at 60 Hz (b).

The rotor resistance was thus estimated by the difference between the locked-rotor resistance and the stator winding resistance $R_s = 158$ mΩ, measured by a *dc* test. The *dc* value for the rotor resistance was obtained by considering the value at lowest frequency reported in Fig. 9c and for all the different machine configurations.

For the considered machine prototype, the no-load and locked-rotor tests with all three-phase sets active (normal conditions) led to the following results:

$$L_m = 18 \, mH, \; L_{cc} = 2.14 \, mH, \; R_r = 159 \, m\Omega \; @ \; 4 \, Sets \; ON \quad (6)$$

The rotor leakage inductance was obtained from the locked-rotor inductance (Fig. 9b) and using the stator leakage inductance evaluated based on [4] ($L_{ls} = 1$ mH).

Fig. 10a reports the measured conventional iron loss profiles obtained using (5). The conventional iron losses are shown at different supply frequencies only in the case of one and four active winding sets to help readability. Their value increases with the frequency for each possible machine configuration. However, according to Fig. 10b, comparing the conventional iron loss profiles in normal conditions (4 sets ON) with those in faulty conditions (1 set ON) at the same supply frequency (60 Hz), they are not overlapped demonstrating that the additional studies are necessary. Also, it is interesting to notice that their variation cannot be scaled by a factor $4/n_{on}$, as observed for the rotor and magnetizing parameters.

The complete maps of the conventional iron losses in function of the supply frequency and stator flux linkage values are shown in Fig. 11.
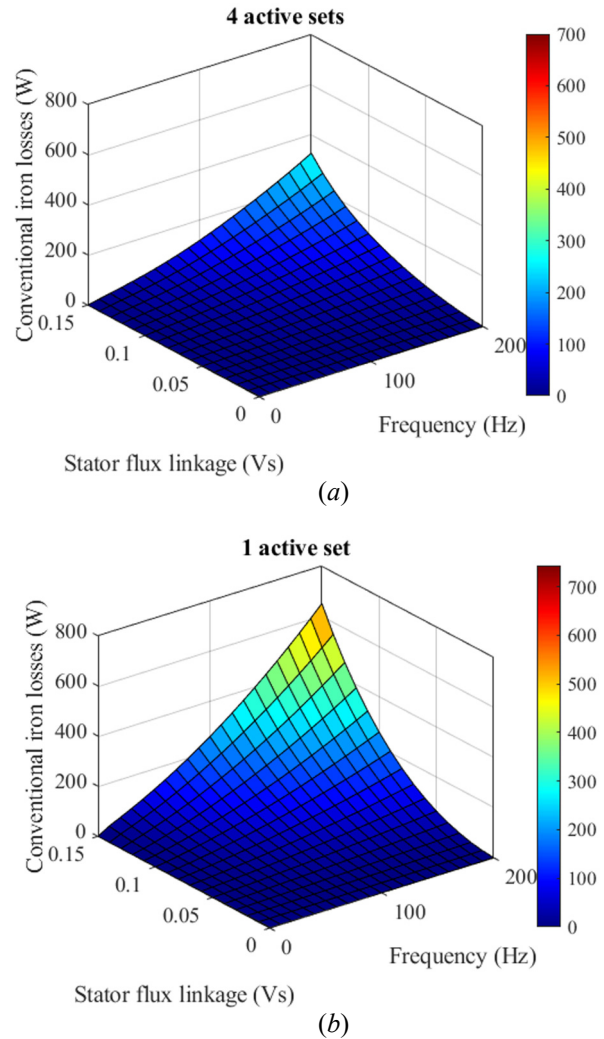

Fig. 11. Experimental iron losses map with four active sets (a) and one active set (b) in function of frequencies and stator flux linkage.

It is noted how the iron losses significantly increase when the machine operates in the worst faulty condition, i.e., one active set. For comparison, it is interesting to observe their maximum value at the rated stator flux linkage of 0.15 Vs and maximum supply frequency of 200 Hz. In the case of one active set, the losses are about 650 W, while in the case of 4 active sets, they are almost halved, i.e., 320 W.

Based on the considerations reported in Section II.A, confirmed by the experimental results, the conventional iron losses modeled with an equivalent iron loss resistance R_{Fe} cannot be simply rescaled in faulty conditions as was done for the rotor magnetizing parameters. An experimental 2D look-up table is thus necessary to accurately map the conventional iron losses for the efficiency evaluation in different load conditions.

IV. PERFORMANCE EVALUATION

The test results obtained in the previous section are used for a preliminary performance evaluation of the machine in different operating conditions, modelling the effects of the magnetic saturation, skin effect and iron losses for all the working points in the torque-speed plane. The efficiency values are computed with a developed efficiency mapping

TABLE VI: MACHINE EFFICIENCY IN NORMAL
AND FAULTY CONDITIONS AT 3000 RPM.

Torque (Nm)	Efficiency			
	4 sets ON	3 set ON	2 sets ON	1 set ON
16	92.7 %	90.4 %	X	X
12	93.1 %	90.8 %	X	X
8	93.2 %	91.6 %	89.0 %	X
4	92.9 %	91.6 %	87.9 %	X
2	92.1 %	90.8 %	87.9 %	85.0 %

procedure for a multi-three-phase machine considering the normal and open-winding fault conditions, similar to the methodology reported in [14]. The mapping provides multiple efficiency maps, solving the equivalent circuit in steady-state conditions, considering the nonlinearities and the machine temperature. The developed mapping also considers the supply voltage and current limits on the maximum torque-per-speed profiles achievable by the machine under analysis, which are heavenly affected by the machine conditions (normal or faulty). Considering that the rated torque on the machine under study is 16 Nm, the efficiencies at 3000 rpm for 100%, 75%, 50%, 25%, and 12.5% of the rated torque were evaluated both in normal and faulty conditions. The efficiency results are reported in Table VI. It is noted how, given a torque-speed point, the efficiency decreases when reducing the number of active sets. However, the obtained results indicate that the efficiency of multi-three-phase machines does not collapse significantly in faulty conditions, highlighting a further advantage of the adoption of multi-three-phase machines. Based on the machine configuration, some working points are not feasible because they are ruled out by the voltage and current limits. Therefore, the maximum deliverable torque of the machine depends on the number of active sets.

V. CONCLUSION

This paper investigated the conventional iron losses, and the saturation phenomena of multi-three-phase induction machines operated in normal and open-winding fault conditions. The MMF distribution in the air gap was investigated, analyzing the harmonic content. In addition, a procedure to identify the parameters of the equivalent circuit of the machine in faulty conditions was proposed. Experimental tests on a 12-phase asymmetrical IM featuring quadruple three-phase stator windings were carried out to accurately estimate the parameters of the equivalent circuit of the machine. Starting from this information, the machine efficiency at various load levels was calculated and compared for different operating conditions, considering both normal and open-faulty conditions.

The reported results highlighted an increment of 50% of the conventional iron losses for the worst considered faulty conditions than the normal one. However, their impact on machine efficiency is not remarkable and can be considered a strength of adopting multi-three-phase machines.

VI. ACKNOWLEDGMENT

VII. REFERENCES

[1] E. Levi *et al.*, 'Multi-phase induction motor drives - a technology status review', *IET Electr. Power Appl.*, vol. 1, no. 4, pp. 489–516, Jul. 2007.

[2] H. A. Toliyat, E. Levi, and M. Raina, 'A review of RFO induction motor parameter estimation techniques', *IEEE Trans. Energy Convers.*, vol. 18, no. 2, pp. 271–283, Jun. 2003.

[3] C. B. Jacobina *et al.*, 'On-line estimation of the stator resistance of a six-phase induction machine', in *Conference Record of the 2002 IEEE Industry Applications Conference. 37th IAS* Annual Meeting (Cat. No.02CH37344*)*, Oct. 2002, vol. 2, pp. 746–751 vol.2.

[4] A. G. Yepes *et al.*, 'Parameter Identification of Multiphase Induction Machines With Distributed Windings—Part 1: Sinusoidal Excitation Methods', *IEEE Trans. Energy Convers.*, vol. 27, no. 4, pp. 1056–1066, Dec. 2012.

[5] S. Rubino, R. Bojoi, M. Mengoni, and L. Zarri, 'Optimal flux selection for multi three-phase machines in normal and fault conditions', in 2017 IEEE IEMDC, May 2017, pp. 1–8.

[6] R. H. Nelson and P. C. Krause, 'Induction Machine Analysis for Arbitrary Displacement Between Multiple Winding Sets', *IEEE Trans. Power Appar. Syst.*, vol. PAS-93, no. 3, pp. 841–848, May 1974.

[7] S. Rubino *et al.*, 'Modular Stator Flux and Torque Control of Multi-Three-Phase Induction Motor Drives', *IEEE Trans. Ind. Appl.*, vol. 56, no. 6, pp. 6507–6525, Nov. 2020.

[8] O. Stiscia, M. Slunjski, E. Levi, and A. Cavagnino, 'Sensorless Control of a Nine-phase Surface Mounted Permanent Magnet Synchronous Machine with Highly Non-Sinusoidal Back-EMF', in IECON 2019, Oct. 2019, vol. 1, pp. 1327–1332.

[9] I. Zoric, M. Jones, and E. Levi, 'Arbitrary Power Sharing Among Three-Phase Winding Sets of Multiphase Machines', *IEEE Trans. Ind. Electron.*, vol. 65, no. 2, pp. 1128–1139, Feb. 2018.

[10] Y. Zhao and T. A. Lipo, 'Space vector PWM control of dual three-phase induction machine using vector space decomposition', *IEEE Trans. Ind. Appl.*, vol. 31, no. 5, pp. 1100–1109, Sep. 1995.

[11] I. Zoric, M. Jones, and E. Levi, 'Vector space decomposition algorithm for asymmetrical multi-phase machines', in *2017 Ee*, 2017, pp. 1–6.

[12] V. Jaiswal and N. K. Deshmukh, 'Determination of iron loss considering spatial harmonics and tooth pulsation effects for cage motor', in *2014 ICRERA*, Oct. 2014, pp. 348–353.

[13] 'IEEE Standard Test Procedure for Polyphase Induction Motors and Generators', *IEEE Std 112-2017 Revis. IEEE Std 112-2004*, pp. 1–115, Feb. 2018.

[14] O. Stiscia, S. Rubino, S. Vaschetto, A. Cavagnino, and A. Tenconi, 'Accurate Induction Machines Efficiency Mapping Computed by Standard Test Parameters', *IEEE Trans. Ind. Appl.*, pp. 1–1, 2022.

VIII. BIOGRAPHIES

Ornella Stiscia (S'19) received the B.Sc. and M.Sc. degrees in electrical engineering in 2016 and 2019, respectively, from Politecnico di Torino, Torino, Italy, where she is currently working toward the Ph.D. degree in electrical engineering in the Department of Energy "G. Ferraris".

Marco Biasion (S'20) received the B. Sc. and M. Sc. degrees in Electrical Engineering from Politecnico di Torino, Torino, Italy. He is currently pursuing the PhD degree in Electrical Engineering at the same university.

Sandro Rubino (S'16, M'18) received the M.Sc. and Ph.D. degrees in Electrical Engineering from Politecnico di Torino, Torino, Italy, in 2014 and 2019, respectively. He is currently Assistant Professor with Dipartimento Energia "G. Ferraris," Politecnico di Torino.

Silvio Vaschetto (S'10–M'13–SM'19) received the M.Sc. and Ph.D. degrees in electrical engineering from the Politecnico di Torino, Italy, in 2007 and 2011, respectively. He is currently an Associate Professor at the Energy Department "G. Ferraris", Politecnico di Torino.

Andrea Cavagnino (M'04–SM'10–F'20) was born in Asti, Italy, in 1970. He received his M.Sc. and Ph.D. degrees in electrical engineering from the Politecnico di Torino, Italy, in 1995 and 2000, respectively. He is a professor at the Politecnico di Torino. He has authored or co-authored more than 250 papers, receiving four Best Paper Awards. Prof. Cavagnino is an Associate Editor of the IEEE TRANSACTIONS ON ENERGY CONVERSION (TEC).

Alberto Tenconi (M'99–SM'10) received the M.Sc. and Ph.D. degrees in electrical engineering from the Politecnico di Torino, Torino, Italy, in 1986 and 1990, respectively. He then joined the Department of Electrical Engineering (now Energy Department), Politecnico di Torino, where he is currently full professor. His research activity is documented by more than 200 papers published in International Journals and International Conferences.